Infectious Disease Modelling 9 (2024) 314–328

Contents lists available at ScienceDirect

Infectious Disease Modelling

journal homepage: www.keaipublishing.com/idm

Unravelling COVID-19 waves in Rio de Janeiro city: Qualitative insights from nonlinear dynamic analysis

Adriane S. Reis [a, b, *], Laurita dos Santos [c], Américo Cunha Jr [d], Thaís C.R.O. Konstantyner [e], Elbert E.N. Macau [a]

[a] Institute of Science and Technology, Federal University of São Paulo, São José dos Campos, SP, Brazil
[b] Physics Institute, University of São Paulo, São Paulo, SP, Brazil
[c] Scientific and Technological Institute, Universidade Brasil, São Paulo, SP, Brazil
[d] Department of Applied Mathematics, Rio de Janeiro State University, Rio de Janeiro, RJ, Brazil
[e] Paulista School of Medicine, Federal University of São Paulo, São Paulo, SP, Brazil

ARTICLE INFO

Article history:
Received 27 September 2023
Received in revised form 23 November 2023
Accepted 21 January 2024
Available online 30 January 2024
Handling Editor: Dr Yiming Shao

Keywords:
COVID-19
Nonlinear analysis
Poincaré plot
Central tendency measure

ABSTRACT

Since the COVID-19 pandemic was first reported in 2019, it has rapidly spread around the world. Many countries implemented several measures to try to control the virus spreading. The healthcare system and consequently the general quality of life population in the cities have all been significantly impacted by the Coronavirus pandemic. The different waves of contagious were responsible for the increase in the number of cases that, unfortunately, many times lead to death. In this paper, we aim to characterize the dynamics of the six waves of cases and deaths caused by COVID-19 in Rio de Janeiro city using techniques such as the Poincaré plot, approximate entropy, second-order difference plot, and central tendency measures. Our results reveal that by examining the structure and patterns of the time series, using a set of non-linear techniques we can gain a better understanding of the role of multiple waves of COVID-19, also, we can identify underlying dynamics of disease spreading and extract meaningful information about the dynamical behavior of epidemiological time series. Such findings can help to closely approximate the dynamics of virus spread and obtain a correlation between the different stages of the disease, allowing us to identify and categorize the stages due to different virus variants that are reflected in the time series.

© 2024 The Authors. Publishing services by Elsevier B.V. on behalf of KeAi Communications Co. Ltd. This is an open access article under the CC BY-NC-ND license (http://creativecommons.org/licenses/by-nc-nd/4.0/).

1. Introduction

Rio de Janeiro, like many other cities around the world, has experienced multiple waves of the COVID-19 pandemic since it first emerged in late 2019 (World Health Organization, 2020). These waves of contagion have had a significant impact on the city's population, healthcare system, and overall way of life (Campos & Canabrava, 2020).

The first wave of COVID-19 in Rio de Janeiro city occurred in early 2020 when the virus was initially detected in the city (Secretaria de Saúde do Rio de Janeiro, 2023). As the number of cases started to rise, strict measures were implemented to

* Corresponding author. Institute of Science and Technology, Federal University of São Paulo, São José dos Campos, SP, Brazil.
E-mail address: adrianereis@usp.br (A.S. Reis).
Peer review under responsibility of KeAi Communications Co., Ltd.

https://doi.org/10.1016/j.idm.2024.01.007
2468-0427/© 2024 The Authors. Publishing services by Elsevier B.V. on behalf of KeAi Communications Co. Ltd. This is an open access article under the CC BY-NC-ND license (http://creativecommons.org/licenses/by-nc-nd/4.0/).

contain the spread (PGE-RJ, 2020). Lockdowns, social distancing guidelines, and travel restrictions were put in place to curb the transmission of the virus. The healthcare system faced significant challenges as hospitals became overwhelmed with COVID-19 patients, leading to shortages of medical supplies and resources.

After several months of restrictions and a decline in cases, Rio de Janeiro city experienced a relative respite from the virus. However, as restrictions eased and people began to return to their normal activities, which gave rise to others waves of contagious. The virus mutations into new variants such as the highly transmissible Gamma, Delta, Zeta and Omicron added an additional layer of complexity to the situation, as they presented new challenges in terms of transmission and vaccine efficacy (Ministério da Saúde, 2021; Giovanetti et al., 2022). Efforts were made to increase testing capacity, contact tracing, and vaccination efforts to mitigate the impact of this waves (Magno et al., 2020). By mid-2021, the city of Rio de Janeiro cautiously started to reopen and return to a semblance of normalcy. However, complacency and the emergence of new variants led to the last big wave of contagion due Omicron variant in late 2021 and early 2022 (Ministério da Saúde, 2023). This wave posed further challenges, as it affected both vaccinated and unvaccinated individuals. Several measures were implemented at that time such as localized lockdowns, capacity limits for businesses, and the promotion of remote work whenever possible (Moura et al., 2022).

Recently, Gianfelice et al. (Gianfelice et al., 2022) analyzed a scenario of multiple waves of COVID-19 in the city of Rio de Janeiro. They were able to distinguish six different waves of contagion by the disease. In this paper, we aim to characterize the dynamics of the six waves of COVID-19 using nonlinear analyses such as Poincaré plot (PP) (Henriques et al., 2020; Tulppo et al., 1996), approximate entropy (ApEn) (Pincus et al., 1991), second-order difference plot (SODP) and central tendency measures (CTM) (Cohen et al., 1996). Poincaré plots are commonly used in time series analysis as a graphical tool to explore and characterize the underlying dynamics of a system, providing a visual representation of the relationship between consecutive data points in a time series, allowing for the analysis of patterns, irregularities, and dynamic properties of the system, being particularly useful in analyzing physiological signals, such as electrocardiograms (ECGs) (Facioli et al., 2021) or electroencephalograms (EEGs) (Chen et al., 2022), offering a valuable approach for time series analysis, enabling the visualization and exploration of the complex dynamics present in the data (Brennan et al., 2001; Karmakar et al., 2009).

Allied to the Poincaré plots, we use approximate entropy, second-order difference plot and central tendency measures to analyze the data series and gain insights into patterns and trends of the six waves of cases and deaths. The approximate entropy is a powerful tool for analyzing time series data (Pincus et al., 1991; Pincus & Goldberger, 1994). By quantifying the complexity and irregularity within a dataset, it helps us to uncover patterns, make predictions, and gain insights into the underlying processes (Delgado-Bonal & Marshak, 2019; Mohseni et al., 2022). The second-order difference plot, also known as the second derivative plot, is a graphical tool used to analyze patterns in a time series, providing insights into the rate of change or acceleration of the underlying data by examining the differences between consecutive data points. However, it is important to note that the interpretation of a second-order difference plot should be done in conjunction with other analysis methods.

We use central tendency measures to assist in interpreting the results obtained with a second-order difference plot. Central tendency measures play an important role in understanding the typical values of a time series and how they change over time (Cohen et al., 1996; Belfort et al., 2019; dos Santos et al., 2015). Represented by a second-order difference plot, this method allows to obtain a comprehensive understanding of a time series allowing us to infer the behavior of the virus spreading and uncover valuable pieces of information from time-dependent data. Our premise is that the dynamics due the different variants, control measures, and vaccination are reflected in the pattern of time series. Therefore, employing these combined analysis will enables us to predict the qualitative behavior of the virus spreading and uncover valuable pieces of information from time-dependent data.

2. Material and methods

Based on the work of Gianfelice et al. which analyzed the scenario of multiple waves of COVID-19 in the city of Rio de Janeiro, we separated the series of cases and deaths data according to the dates specified by the authors (Gianfelice et al., 2022).

The analyzed time series corresponds to the period from March 3, 2020 to September 9, 2022 in Rio de Janeiro (RJ) city, Brazil. Given the significant fluctuations present in the time series of cases and deaths, stemming directly from the disease and deficiencies in the surveillance system, the raw data was smoothed using a 7-day moving average. The data was obtained by aggregating information collected by the responsible organizations in an extensive spreadsheet that contains various details, such as zip code, date of first symptoms, type and date of outcome (recovery or death), among others. It is worth mentioning that although the mentioned information was present in the spreadsheet, the patients identities were not revealed. The mentioned data was registered by the municipal health authorities and is available for consultation on the Rio COVID-19 Panel (EpiRio, 2023).

During the period considered we set only six waves of contagion: 1st wave (Mar 03, 2020 to July 17, 2020); 2nd wave (July 17, 2020 to Nov 06, 2020); 3rd wave (Nov 06, 2020 to Mar 01, 2021); 4th wave (Mar 01, 2021 to July 08, 2021); 5th wave (July 08, 2021 to Dec 11, 2021); 6th wave (Dec 11, 2021 to Sept 09, 2022). Fig. 1 show the time series for cases and deaths caused by COVID-19. These dates are close, but not identical to the dates presented in (Gianfelice et al., 2022), which were determined by data-assisted curves. Here, similarities in subsets of the time series are taken into account to determine the start and the end dates of each wave, using the dates of (Gianfelice et al., 2022) as a reference.

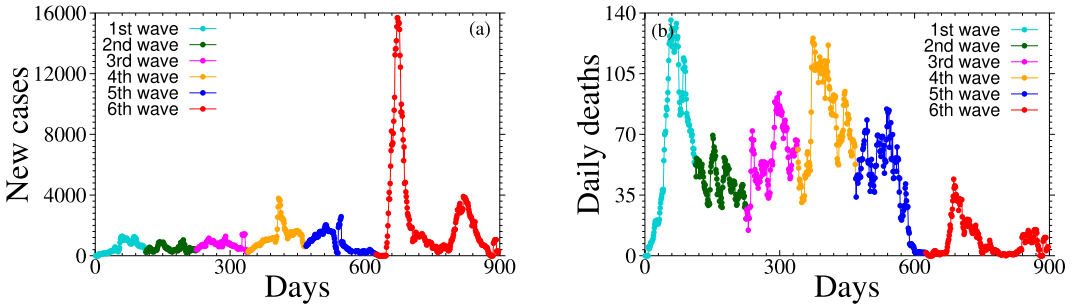

Fig. 1. Time series for new daily cases (a) and deaths (b) of COVID-19 considering a seven-day moving average. The colors represent the six different waves that occurred in the city of Rio de Janeiro: 1st (turquoise), 2nd (green), 3rd (magenta), 4th (orange), 5th (blue) and 6th (red).

In both time series, the onset and end of the waves were considered as described above, from March 2020 to September 2022. Each color represents a wave: 1st (turquoise), 2nd (green), 3rd (magenta), 4th (orange), 5th (blue), and 6th (red). For simplicity and comparison purposes, the colors and dates of the waves for cases and deaths were considered the same.

2.1. Poincaré Plot

Poincaré plots, also known as first return maps or Poincaré maps, are graphical tools used to analyze the dynamics of a complex system. For time series, Poincaré plot is a widely used method to analyze the correlation between time series. Generally, Poincaré plots have been employed to analyze heart rate variability and identify abnormalities in cardiac dynamics (dos Santos et al., 2013; Brennan, Palaniswami, & Kamen, 2002; Koichubekov et al., 2017; Facioli et al., 2021). The construction of a Poincaré map is done on a geometric representation of a data series, in which the consecutive points of the time series are plotted. Each interval in the considered time series is a function of the previous interval, therefore, it returns a recurrence measure that reflects the correlation between successive intervals of a time series (Brennan et al., 2002). Graphically, the duration of a current event is displaced in axis x_i and the following event in the x_{i+1}.

One way to quantify the dispersion of emergent pattern that appears in the PP is by measuring the descriptors SD_1 and SD_2. These descriptors are defined by the standard deviation perpendicular to the line of identity (SD1) and the standard deviation parallel to the line of identity (SD2) (Hsu et al., 2012) and calculated by fitting an ellipse according to the dispersion of points in the shape of Poincaré plot (Brennan et al., 2001; Karmakar et al., 2009; Tulppo et al., 1996). In general, they represent the variation of short and long and term that allows a guided visual inspection of the distribution of points. Is important to mention that these measures are linear statistics and, therefore, do not directly quantify the temporal nonlinear variation, so it is interesting to use different delays in order to capture changes resulting from this variation in the delayed time (Koichubekov et al., 2017; Satti et al., 2019).

2.2. Approximate entropy

Generally, the measurement of entropy in well-defined physical systems is done by the Kolmogorov-Sinai entropy (K–S) (Kolmogorov, 1959). However, the K–S entropy has some limitations which makes this measure not the best choice for analyzing certain types of systems. For complex systems whose time series present a lot of noise and fluctuations, the K–S entropy measurement does not give satisfactory results, requiring the implementation of other methods capable of circumventing these limitations (Delgado-Bonal & Marshak, 2019). Some methods were developed, based on K–S entropy, to solve these problems. When dealing with the analysis of a data series that presents many fluctuations, or a series generated by an unknown system, a widely used method to measure entropy is the calculation of the approximate entropy (Pincus, 1991; Pincus et al., 1991).

ApEn is a statistical measure used to quantify the complexity or irregularity of time series data. It was originally introduced by Pincus in 1991 (Pincus, 1991) as a tool for assessing the regularity or predictability of physiological signals, such as electroencephalography (EEG) and heart rate variability (HRV) (Pincus et al., 1991; dos Santos et al., 2013). The calculation of approximate entropy involves comparing subsequences within the time series data and quantifying the similarity between them. The algorithm measures the logarithmic likelihood that subsequences of a certain length (m) will remain similar when the data is expanded to include an additional data point (Delgado-Bonal & Marshak, 2019). This process is repeated for different subsequence lengths and compared to assess the complexity of the data. The approximated entropy is as follows

$$ApEn(m, R) = \Phi(m+1, R) - \Phi(m, R), \tag{1}$$

where m is the length of the compared subsequences, R is the tolerance or similarity criterion used to determine whether two subsequences are considered similar. $\Phi(m, R)$ is the average logarithmic probability that two subsequences of length m match within a tolerance R.

Low approximated entropy values indicate that the system is repetitive, persistent and predictive, presenting patterns that are repeated throughout the analyzed time series. On the other side, high values indicate independence between the data (low correlation), a low number of repetitive patterns, and some randomness (Delgado-Bonal & Marshak, 2019; Pincus & Goldberger, 1994). It is important to note that, although ApEn is calculated by a change in K–S entropy, it is not an approximation of this entropy measure. ApEn returns a statistical measure of the degree of regularity and unpredictability in a time series, that is, it does not serve to determine the dynamics of a system completely, but to classify them and study the evolution of their complexity. Thus, the ApEn measure may be used as an indicative method of small changes in the dynamics of a time series.

2.3. Central tendency measure and second-order difference plot

The CTM method measures the variability of data in a time series, in which successive differences are plotted against each other (Cohen et al., 1996; dos Santos et al., 2015). In addition to showing the variability present in the time series, the graph resulting from this plot also shows nonlinear aspects in the sequence of the series in the time intervals considered. The correlation of the time series data is computed in the SODP from the difference of the two variables analyzed by the co-ordinates $(x_{i+1} - x_i)$ and $(x_{i+2} - x_{i+1})$, where each sample value x_i denotes an interval x in time i.

This method is an effective tool for quantifying the level of variability computed by the SODP. We compute the CTM from the data time series by selecting a circular region of radius R around the origin, taking into account the ration of the number of points that falls within the regions delimited by the radius R and the total number of points (Abásolo et al., 2006; Altan et al., 2019)

$$\mathrm{CTM} = \frac{\sum_{i=1}^{N-2} \delta(d_i)}{N-2}, \tag{2}$$

being $\delta(d_i)$ defined as

$$\delta(d_i) = \begin{cases} 1, & \text{if } [(x_{i+1} - x_i)^2 + (x_{i+2} - x_{i+1})^2] < R, \\ 0, & \text{otherwise.} \end{cases}$$

Low values of CTM, for a specific R, indicate a few points within the circle. If a larger radius is needed to include all points on the SODP, this is an indication of high variability in the series (dos Santos et al., 2015). In summary, a low CTM value indicates a large dispersion and a high value indicates concentration close to the center, that is, the higher the CTM, the smaller the variability.

3. Results and discussion

In this section, we present the discussions of the results obtained by applying the methods mentioned in the previous sections to describe the qualitative behavior of the propagation of cases and occurrences of deaths caused by SARS-CoV-2 (severe acute respiratory syndrome).

3.1. Poincaré plot analysis

At first, we will analyze the qualitative behavior of the number of new cases of COVID-19 infection in the city of Rio de Janeiro. The time series used comprise the same waves of cases shown in Fig. 1(a). As mentioned in Sec. 2.1 it is interesting to analyze the dynamics of contagion by the disease at different times, in this way, we will achieve a better qualitative description of the dynamics of propagation of the disease. Fig. 2 illustrates Poincaré plot for the evolution of daily cases for each wave of COVID-19 as time varies from $\tau = 1$ to $\tau = 5$, to capture the temporal nonlinear variation (Koichubekov et al., 2017; Satti et al., 2019).

A visual inspection of the first panel in Fig. 2, corresponding to the 1st wave ($\tau = 1$), the PP reveals the presence of several points concentrated along the identity line ($x_{i+1} = x_i$). This indicates that at the onset of the disease, there is a strong correlation in the number of new cases per day. We should recall that when dealing with epidemiological diseases, there is a time in which the symptoms of the disease take to manifest in the infected individual (virus latency period). Overnight, the initially infected group contaminates another group due to people interactions, which, in turn, infects a new group of individuals, starting community transmission. Such behavior can be observed by the increasing number of new cases. We should pay attention to the fact that, concerning the first wave, we are at the beginning of the pandemic in Rio de Janeiro city. During this period, the restrictions on the movement of people had not yet been widely adopted by a significant portion of the population since the 1st decreet was on March 11, 2020 (PGE-RJ, 2020). As time passes, we observe that the time series begins to lose correlation. This could indicate that the initially infected group has acquired immunity, at least to the same variant circulating during this period.

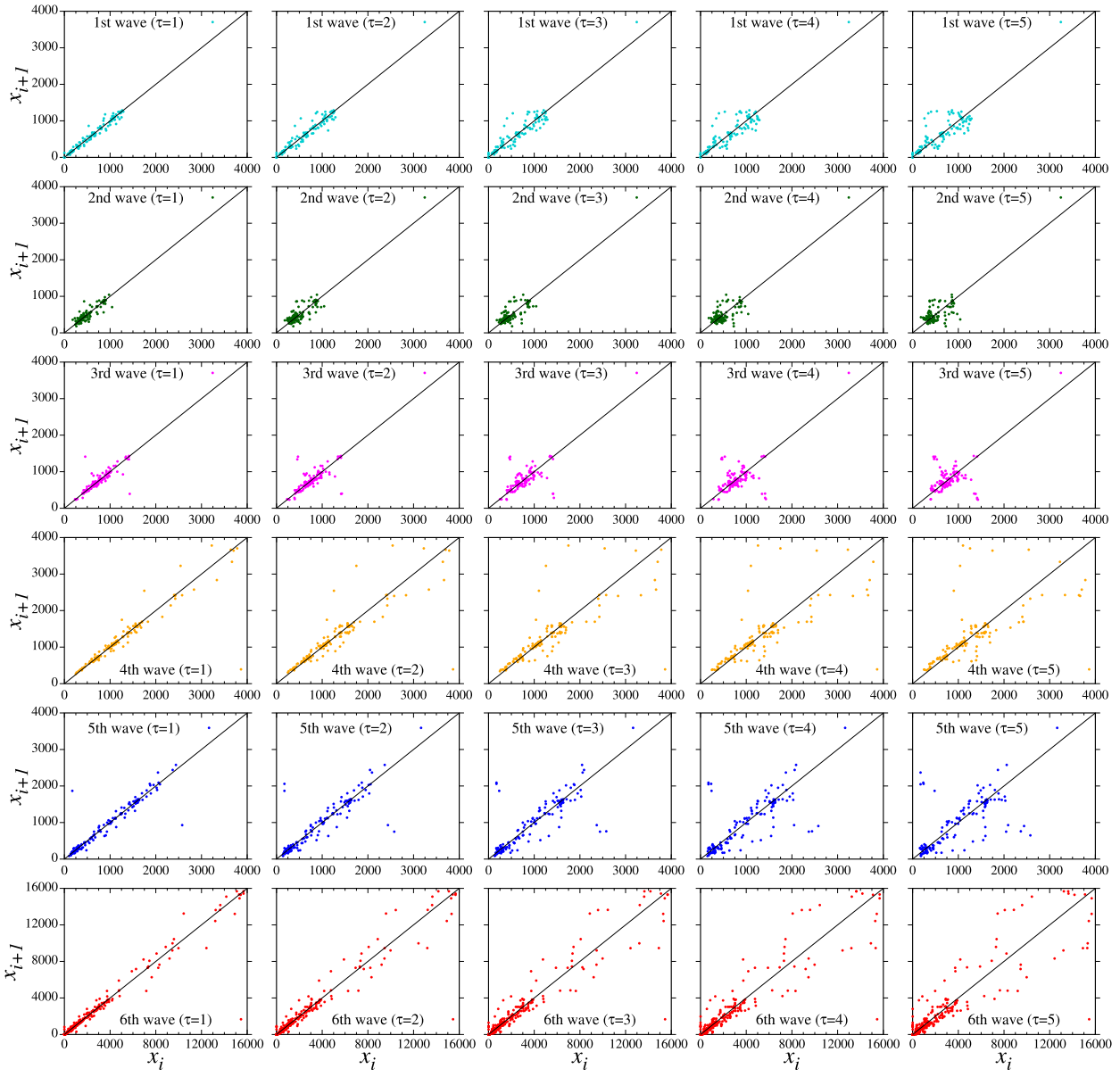

Fig. 2. Poincaré plot for occurrence of cases with different values of τ. All frames were placed on the same scale, except for the 6th wave. By direct observation, it can be seen that as the value of τ increases in the Poincaré graph, the correlation between the points decreases.

That being so, the initial high correlation observed in the PP during the 1st wave can be analyzed in terms of an initial population of infected individuals who, due to the virus's latency period and the absence of symptoms, end up infecting susceptible individuals. As the system evolves over time, for $\tau = 2$, it can be noticed that some points start to become more dispersed in the PP, indicating a slight decrease in the correlation of new cases for the first wave. As we vary τ from 1 to 5, the loss of correlation from one day to the next becomes more evident. When $\tau = 5$, the correlation of new cases decreases significantly, and the geometric representation of the PP approaches the shape of the system attractor. This decline in correlation over time suggests that as individuals acquire immunity to the current variant or due to reduced contact between the population of infected and susceptible individuals (social isolation), the number of new daily cases tends to decrease.

In the 2nd wave, we observe that the number of new cases per day is slightly lower compared to the 1st wave. As seen in the PP, the time series it describes exhibits a shortening along the diagonal and the presence of more scattered points perpendicular to the identity line. This suggests that during the considered period, short-term contagion is less responsible for the number of cases. Thus, considering that the number of cases was lower compared to the 1st wave, it can be conjectured that during this period, individuals remained infected for a longer time or stayed asymptomatic for a longer time.

A similar behavior is observed for the time series of the 3rd wave. In this case, the number of new cases per day is higher compared to the 2nd wave. However, as we vary τ, the correlation of the time series decreases. It is interesting to note that in both the 2nd and 3rd waves, there is a region of "separation" of some points, forming a cluster close to the region with higher correlation. By analyzing the geometric pattern in Fig. 2, this can indicate a long-term loss of correlation associated with a short-term one. In other words, a period in the time series during which the number of new cases remained approximately constant.

The fourth wave is characterized by an initial pattern with numerous points along the identity line, indicating a high correlation. However, there is also a pattern where the points are more scattered away from the identity line, perpendicular to it. Analyzing the time series in Fig. 1(a), we can observe a sudden increase in the number of cases, which is captured by the emergence of a new cluster in the PP. Similar to the previous waves, the points are dispersed perpendicular to the identity line, suggesting that short-term contagion is not solely responsible for the increase in cases. During the 4th wave, Brazil experienced a significant increase in cases due to the predominant circulation of the Gamma variant (since January 2021), a variant of concern (VOC). In the same period, in the city of Rio de Janeiro, the Zeta variant (P.2), a mutation of the Gamma variant (variant of interest - VOI), was responsible for a significant rise in daily new infections. The Gamma variant can be 1.7 to 2.4 times more transmissible than other VOCs, indicating that short-term contagion was not the primary factor contributing to the pronounced increase in cases. Rather, the mutation of the virus played a crucial role (Ministério da Saúde, 2021; Ministério da Saúde, 2023; Giovanetti et al., 2022).

An equivalent pattern can be observed for the 5th wave; however, the geometric representation of the time series in the Poincaré plot exhibits a slight shortening along the diagonal. This suggests that, in addition to the number of daily cases being lower than in the 4th wave, there is a higher correlation between short-term and long-term variabilities, considering the spread of the disease. The variations in correlation around the central part are due to the oscillations shown in the time series, where there is a reduction in the number of new cases (explaining the scattered points in the lower part of the plot), followed by a subsequent increase in the number of cases.

Lastly, the 6th wave corresponds to the period when the Omicron variant was circulating in Brazil. The main characteristics of the Omicron variant (B.1.1.529) include a higher reinfection rate compared to other VOCs and milder symptoms, which can lead an infected individual to not identify the infection caused by the virus (Ministério da Saúde, 2021; Ministério da Saúde, 2023). Analyzing the PP, when $\tau = 1$, we can see different clusters in the dispersion pattern of points. At the beginning of the 6th wave, the points are highly correlated, indicating low variability in the number of new cases from one day to the next. After a certain period, there is a break in this geometric pattern, and the first cluster emerges, revealing the abrupt increase in the number of new daily COVID-19 cases. Once again, the presence of other clusters indicates a decrease and subsequent increase in the number of cases. Finally, the PP shows reduced variability, indicating that up until the considered period, daily cases tend to stabilize around a constant value.

It is interesting, in this case, to mention the effects of increasing τ for the study of the time series. As we increase τ, we observe the same pattern of clusters; however, the variability within each cluster necessarily decreases, approaching the system's attractor. Note that waves 1 to 5 were all shown on the same scale, except for the 6th wave, which had the highest number of daily cases. Overall, this behavior can be observed for all the waves considered in this study, with slight variations for each of them.

The analysis of the PP allows a qualitative representation of the dynamics of COVID-19 waves. One way to quantify these results is by using the measures of the descriptors SD_1 and SD_2, as discussed in Sec. 2.1. Table 1 presents the values of the descriptors SD_1, SD_2, and the ratio between them. By observing the values of these descriptors, we can see that they corroborate the results obtained from the figures shown on the Poincaré map (Fig. 2), where we observe a breakdown of correlation within each wave as we increase the values of τ.

Considering the 1st wave, we can see that the calculated values for SD_1 and SD_2 align with the results obtained from the PP. When $\tau = 1$, the SD_1 measure has the lowest value. As τ increases, the value of SD_1 increases, reflecting the loss of correlation observed in the first frame of Fig. 2. Regarding SD_2, there is little variation in the calculated values, suggesting that long-term variability is not a determining factor in the first wave. The ratio of the descriptors provides the day-to-day variation of the number of cases according to the variation of SD_1 relative to SD_2. According to Table 1., for $\tau = 1$, $SD_1/SD_2 = 0.15$ (1st wave), indicating that there is not much variation between the measures, thus corroborating the correlation observed in the PP.

In the 2nd wave, the most pronounced characteristic is the shortening of the diagonal (identity line), and the value of SD_2 captures this behavior well when compared to the 1st wave, as we can see that these values are lower. The values of SD_1 follow the same pattern as in the previous case, where correlation decreases as τ increases, consequently leading to an increase in SD_1. The ratio between the descriptors, in the case of the 2nd wave, is almost twice as high as in the 1st wave, reinforcing the idea that during this period, people remained infected for a longer time, as the day-to-day variability is higher in this period. In the period corresponding to the 3rd wave, the values of SD_1 and SD_2 are consistent with what is shown in Fig. 2. The value of $SD_1/SD_2 = 0.43$ captures the points off the diagonal in the PP, indicating appreciable long-term and short-term variation in the time series of COVID-19 cases during this period. Overall, the results presented in Table 1 corroborate the observed behavior in the PP, revealing the loss of correlation as τ increases.

The same quantitative and qualitative analyses were conducted for the time series of COVID-19 deaths, considering the same intervals for the beginning and end of the waves. In order to facilitate visual comparison, the colors representing the waves have been kept consistent. The analysis of the PP of the six waves of deaths from COVID-19, as shown in Fig. 3, reveals patterns similar to those observed in cases time series.

Table 1
Values of SD_1, SD_2 and ratio for occurrence of cases of COVID-19 for τ varying from 1 to 5.

1st wave	τ_1	τ_2	τ_3	τ_4	τ_5
SD_1	40.58	65.89	87.40	107.92	124.71
SD_2	265.77	261.52	255.20	248.28	240.68
SD_1/SD_2	0.15	0.25	0.34	0.43	0.52
2nd wave	τ_1	τ_2	τ_3	τ_4	τ_5
SD_1	52.41	65.02	73.14	85.60	92.76
SD_2	161.10	157.30	156.28	151.39	144.12
SD_1/SD_2	0.32	0.41	0.47	0.56	0.64
3rd wave	τ_1	τ_2	τ_3	τ_4	τ_5
SD_1	96.91	128.04	152.15	171.90	190.09
SD_2	255.33	215.81	199.38	185.76	163.17
SD_1/SD_2	0.43	0.59	0.76	0.92	1.16
4th wave	τ_1	τ_2	τ_3	τ_4	τ_5
SD_1	89.27	166.40	233.11	287.61	333.02
SD_2	713.86	700.32	680.32	657.91	633.43
SD_1/SD_2	0.12	0.24	0.34	0.44	0.53
5th wave	τ_1	τ_2	τ_3	τ_4	τ_5
SD_1	138.08	199.22	240.77	266.12	295.93
SD_2	431.65	417.18	398.50	387.09	366.45
SD_1/SD_2	0.32	0.48	0.60	0.69	0.81
6th wave	τ_1	τ_2	τ_3	τ_4	τ_5
SD_1	271.11	415.80	563.85	700.63	834.17
SD_2	3591.21	3582.22	3568.22	3548.03	3524.61
SD_1/SD_2	0.07	0.12	0.16	0.20	0.24

In the 1st wave, we can see a geometric pattern similar to what was observed in the 6th wave of cases. The PP shows low variability initially, followed by the emergence of clusters due to the increase in the number of deaths over the considered period. As we increase τ, the points become more dispersed, indicating a decrease in correlation. In the subsequent waves (2nd, 3rd, 4th, 5th, and 6th), a similar behavior is observed in the PP for deaths. In the 2nd wave of deaths, we observe a similar shortening of the diagonal as in the cases time series. During this period, it is assumed that individuals manifested the symptoms of the disease later, remaining infected for a longer time. The number of deaths is lower in the 2nd wave compared to the 1st wave because some of the individuals infected during this period only started showing symptoms in the interval that corresponds to the 3rd wave. In both the PP and the death time series, we can observe an increase in the number of deaths during the 3rd wave. As seen in the PP, the time series corresponding to the 3rd wave exhibits the appearance of clusters related to the abrupt increase and decrease in the number of deaths.

The dynamics of the 4th wave of cases differs significantly from that of deaths. While in the former, the loss of correlation is evident, for deaths, the correlation is still appreciable. However, as τ increases, the dispersion occurs around the diagonal without the formation of clusters, indicating that the number of deaths is slightly decreasing (without many abrupt variations) along the time series, exhibiting greater variability of points perpendicular to the identity. In other words, the effect is more apparent in the short term. The behavior of the 5th wave is similar to the pattern observed in the previous period, revealing the predominance of short-term variation and a decrease in the number of deaths in the time series.

During the 6th wave, we once again observe the shortening of the PP. The number of deaths has decreased considerably compared to the previous waves. It is noteworthy that the plot shows a low variability of points, indicating a strong correlation between short and long-term. Additionally, we observe the emergence of a cluster, which, combined with the high correlation seen in the PP, indicates a period of stability in the number of cases, followed by a further decrease in the number of deaths (Fig. 1(b)). The hypothesis is that this behavior may be associated with the effects of the advanced vaccination campaign among the population at this stage.

The SD_1 and SD_2 descriptors, as well as their ratio, were calculated for the death time series (Table 2). The values obtained provide quantitative measures of the variability and correlation in the data.

The results presented in Table 2 further support the findings from the PP, confirming the decreasing correlation as τ increases. The measure of the diagonal (SD_2) shows slight variations as we increase the value of τ, with the highest value observed in the first wave. It is worth noting that for the second wave, the value of SD_2 decreases considerably, reflecting the shortening of the diagonal observed in the PP. The quantity SD_1/SD_2 is lower than for the cases, suggesting that for deaths, there is no significant distinction between long-term and short-term variables, except in the second wave where $SD_1/SD_2 = 0.30$ (2nd wave), which is the highest variation captured for deaths.

The contrasting results between the number of cases and deaths are due to the Omicron variant circulating in the city of Rio de Janeiro during this period, which, despite its high transmission, has a low mortality rate, either due to acquired immunity from previous infections or the effect of vaccination. It is interesting to note that for both cases and deaths, as we consider $\tau > 1$, the time series loses correlation. This indicates that the disease tends to stabilize, meaning that either the

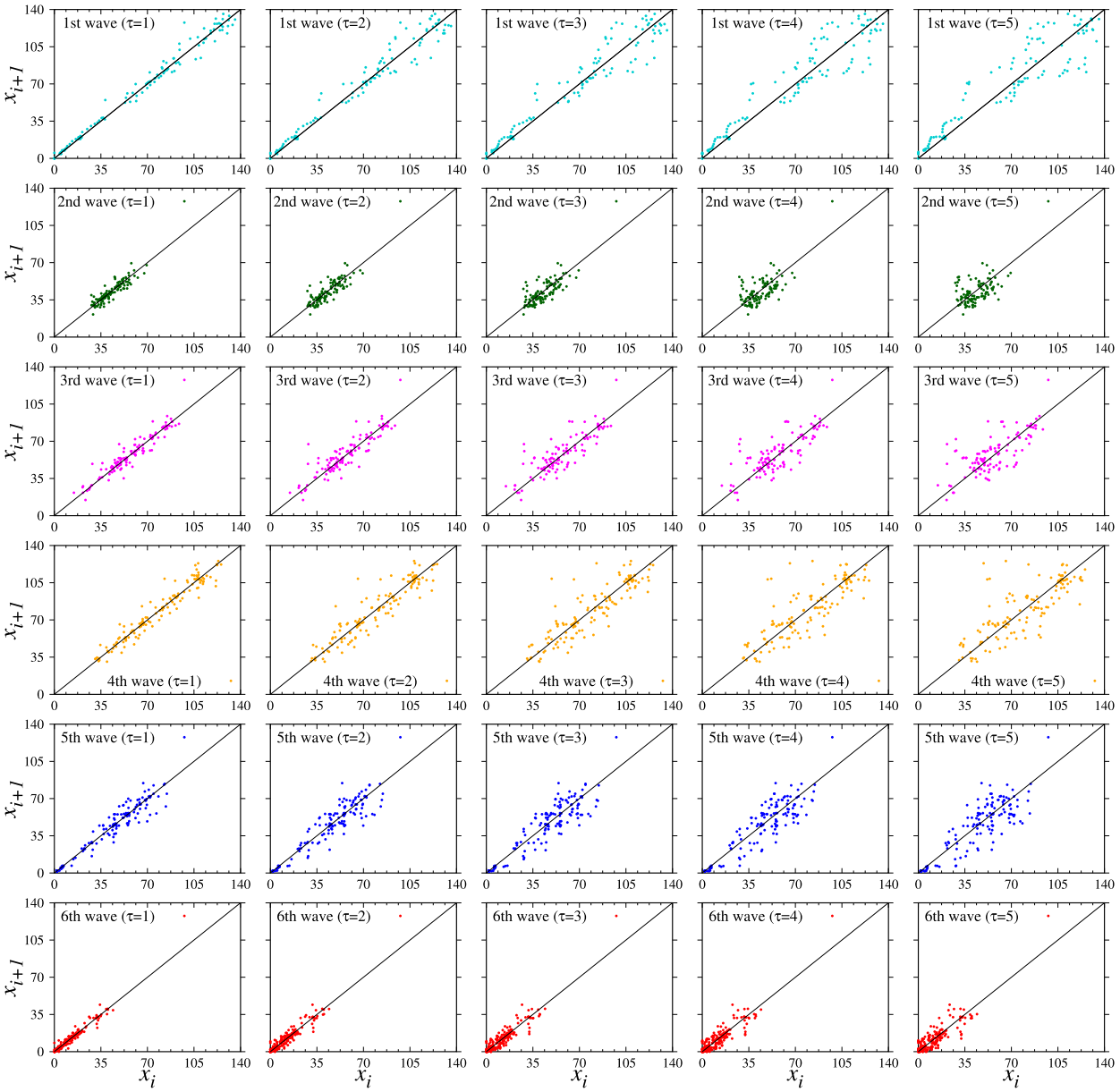

Fig. 3. Poincaré plot for occurrence of deaths with different values of τ. All frames were placed on the same scale, except for the 6th wave. By direct observation, it can be seen that as the value of τ increases in the Poincaré map, the correlation between the points decreases.

number of cases remains at a constant rate or the infection through virus transmission is extinguished, either through the implementation of control measures, acquired immunity, or the action of vaccines. Therefore, considering the COVID-19 pandemic, and likely other epidemic diseases with similar spreading patterns, as time goes on, the observed behavior between cases and deaths becomes inverse.

3.2. Approximate entropy analysis

The result illustrated in Fig. 4 shows how the measure of ApEn varies, considering different values for R, in the time series of cases. By inspection of Fig. 4, we see that the 2nd wave has the highest entropy value (ApEn ≈ 0.80) while the 4th has the lowest value (ApEn ≈ 0.42) with $0 \leq R \leq 6.3 \times 10^3$. As the value of the parameter R increases, the entropy values decrease, until it reaches zero, which indicates that the data series becomes more predictable, that is, the system reaches a state of equilibrium. The amplification in Fig. 4 allows better visualization of the entropy behavior for each series.

Table 2
Values of SD_1, SD_2 and ratio for occurrence of deaths of COVID-19 for τ varying from 1 to 5.

1st wave	τ_1	τ_2	τ_3	τ_4	τ_5
SD_1	2.57	4.21	5.44	6.58	7.72
SD_2	29.90	29.63	29.22	28.77	28.33
SD_1/SD_2	0.08	0.14	0.19	0.23	0.27
2nd wave	τ_1	τ_2	τ_3	τ_4	τ_5
SD_1	2.02	2.53	3.08	3.79	4.26
SD_2	6.84	6.74	6.58	6.14	6.06
SD_1/SD_2	0.30	0.37	0.47	0.62	0.70
3rd wave	τ_1	τ_2	τ_3	τ_4	τ_5
SD_1	2.89	4.00	4.93	5.78	6.53
SD_2	14.62	14.48	14.17	13.87	13.60
SD_1/SD_2	0.20	0.28	0.35	0.42	0.48
4th wave	τ_1	τ_2	τ_3	τ_4	τ_5
SD_1	3.43	4.91	6.28	7.51	8.68
SD_2	17.67	17.63	17.86	17.83	17.79
SD_1/SD_2	0.19	0.27	0.35	0.42	0.49
5th wave	τ_1	τ_2	τ_3	τ_4	τ_5
SD_1	3.49	4.25	4.52	4.82	5.70
SD_2	17.87	17.48	17.21	17.03	16.72
SD_1/SD_2	0.19	0.24	0.26	0.28	0.35
6th wave	τ_1	τ_2	τ_3	τ_4	τ_5
SD_1	1.16	1.58	1.96	2.34	2.68
SD_2	8.46	8.42	8.38	8.34	8.29
SD_1/SD_2	0.14	0.19	0.23	0.28	0.32

The waves with the lowest ApEn values are 1, 4, and 6. Looking at the behavior of the 1st wave in Fig. 2 ($\tau = 1$), a relationship can be seen between the entropy value and the results obtained by the PP. Given the high correlation present in the first wave, suggested by the first return map, the pattern of the time series is more predictable, which implies a lower variability of the time series and, therefore, low ApEn. The same behavior is seen in waves 4 and 6, both have low ApEn, which indicates little variability during the considered periods.

During the fourth wave, the transmission of the virus by the Zeta variant was predominant in the city of Rio de Janeiro, although this variant was responsible for an increase in the number of cases, the spread of the virus occurred similarly to the 1st wave. For the 6th wave, the behavior is similar to that presented by waves 4 and 5. Again, the approximate entropy value indicates a more predictable pattern of the time series. The ApEn calculation reveals the low complexity in the time series caused by the transmission of the virus due to the variants Alpha (B.1.1.7), Zeta (P.2), and Mu (B.1.621), each of which captures the effects of the restraint measures adopted in the periods in question.

The 2nd, 3rd, and 5th waves achieve the highest values of approximate entropy. In the case of the 2nd wave, as observed in the PP, the time series exhibits a less predictable pattern, with scattered points along the diagonal and the formation of clusters. This indicates that the patterns are less repetitive, leading to higher complexity and, consequently, higher entropy values in the time series. The low predictability of the time series in the 2nd wave may be associated with the characteristics of the Gamma variant. As mentioned earlier, individuals take a longer time to develop symptoms, which leads to delays in

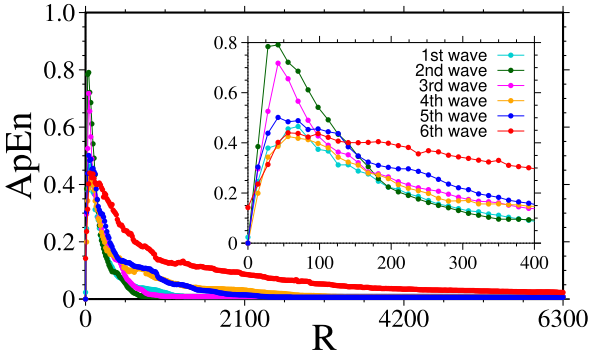

Fig. 4. Approximated entropy for incidence of new cases. Each color corresponds to one wave. The amplification shows a better visualization of the entropy for each series.

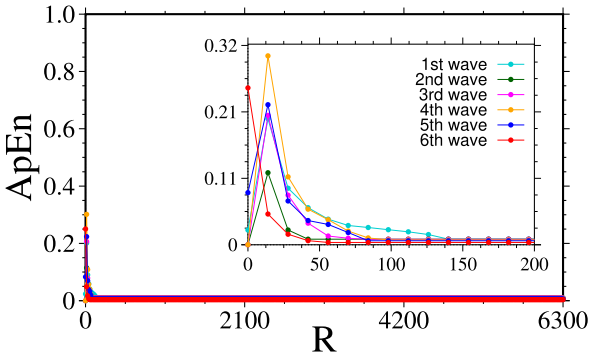

Fig. 5. Approximated entropy for incidence of daily deaths. Each color corresponds to one wave. The amplification shows a better visualization of the entropy for each series.

implementing restrictive measures. All of these factors contribute to an increase in the number of cases, which is subsequently captured in the 3rd wave.

Regarding the 5th wave, combining the results of approximate entropy with those obtained from the PP, we observe that most points lie along the diagonal, indicating a good correlation between the data. However, the presence of scattered points away from the identity line and the formation of clusters increase the variability of the data. This results in an approximate entropy value of around 0.5, indicating the simultaneous presence of regularity and unpredictability in this period.

The behavior of the third wave is similar to that of the second wave, exhibiting a less predictable pattern. This is captured by the presence of clusters, indicating higher variability in the data. As for the fifth wave, it has an intermediate approximate entropy value (around 0.5). When analyzing it together with the PP, we observe the presence of clusters with good correlation and less repetitive patterns.

Analyzing the time series of deaths (Fig. 5), the initial observation is that the value reached for the entropy of the COVID-19 waves. Comparing the entropy values for deaths with those for cases, we can see that all the entropy values for deaths are lower. In Fig. 5, we can observe that the maximum entropy value is approximately ApEn ≈ 0.31 for the 4th wave, and the minimum value is approximately ApEn ≈ 0.12 for the 2nd wave. These values are directly related to the dynamics of virus spread.

In the 2nd wave, there was an increase in the number of cases caused by the Gamma variant, which resulted in a high number of deaths during that period, making the time series more predictable. On the other hand, the 4th wave shows higher entropy values, capturing the effects of the start of the vaccination campaign, indicating that the number of individuals who die is lower than the number of infections. This result can be confirmed by comparing the entropy for the cases (Fig. 4) *vs* deaths time series (Fig. 5) during the 4th wave period.

The results of entropy indicate that the time series of deaths exhibits lower complexity compared to the time series of cases. This is expected since deaths have more deterministic dynamics, as they are directly related to confirmed cases that have progressed to death. Unlike cases, where the dynamics of virus spread can be influenced by various factors such as control measures, incubation period of the disease, and characteristics of circulating variants, deaths are directly linked to the clinical outcome of infected individuals. Therefore, it is natural for the time series of deaths to be more predictable and exhibit lower complexity than the time series of cases. The slight differences in the entropy values shown in Fig. 5 are due to the fact that the number of deaths varies from one wave to another. This can be corroborated by the SD_1 measurements, where it can be observed that the long-term variation does not show significant changes. For the time series of deaths with $\tau = 1$, similar to what occurs with cases, as R increases, the entropy value tends to zero, indicating that the disease reaches a state of equilibrium.

3.3. Central tendency measure analysis

The results shown below were obtained using the SODP and CTM. Fig. 6 displays the relationship between CTM and radius (R) for the cases of COVID-19. It can be observed that as the radius value increases, all the points tend to fall within the radius R, causing the CTM value to saturate at 1. Given this, we choose a radius that provides intermediate CTM values. The CTM is evaluated on a range from 0 to 1, so as R increases, it is expected that the CTM value saturates at 1, indicating that all the points are within the specified radius.

Fig. 6 illustrates the CTM value for each wave as the radius varies. In the second-order difference plot, a radius of $R = 200$ was set for waves from 1 to 5, and $R = 400$ for the 6th. This choice of radius allows for an appropriate representation of the waves in the second difference plot.

We can observe that for $R > 400$, five waves exhibit a high CTM value, indicating low variability. In these cases, all the points fall within the radius. However, the 6th wave stands out with a CTM value of approximately 0.7, indicating greater variability than the other waves. This shows that the series of the 6th wave has more scattered points outside the radius.

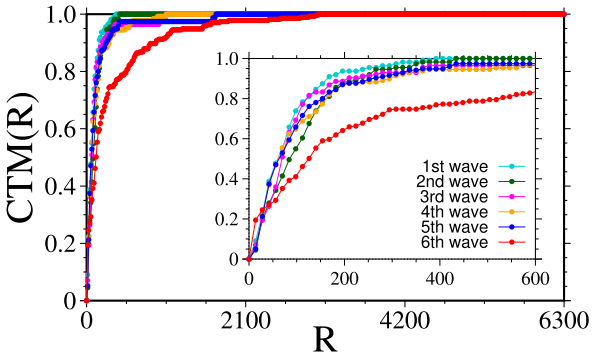

Fig. 6. Variation of CTM by radius for time series of cases. As R increases, all waves tend towards CTM = 1.

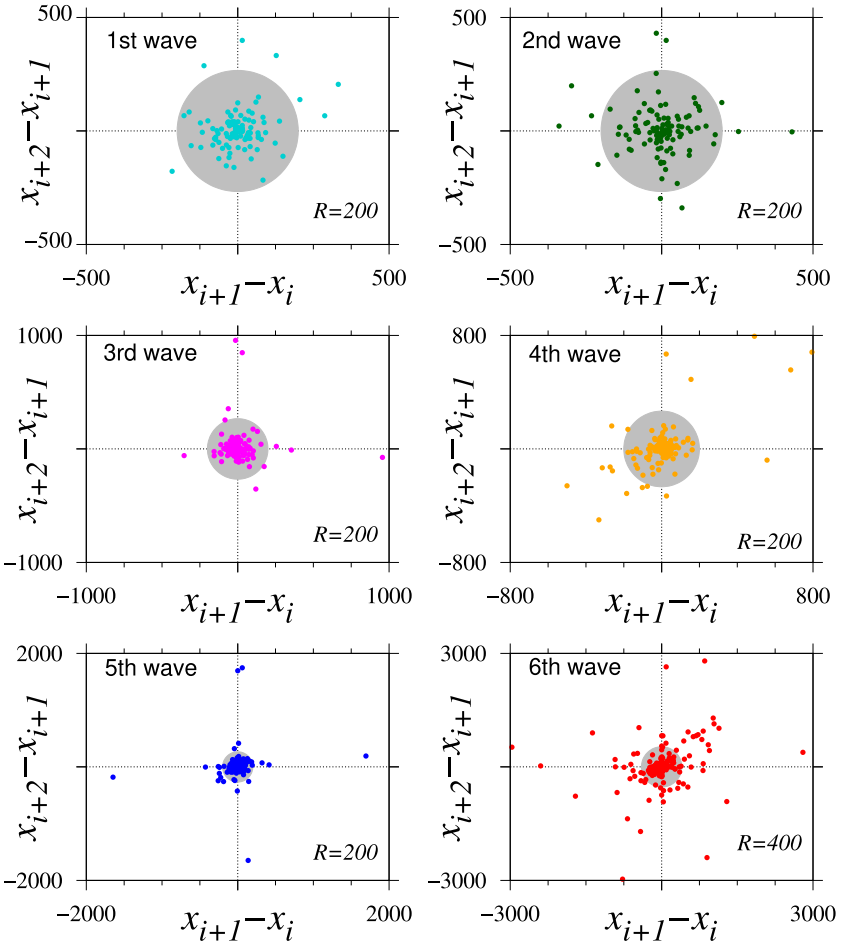

Fig. 7. Second-order difference plot for the six waves of COVID-19 cases. It is possible to distinguish the behavior of each wave by the rate of the virus spreading speed.

The SODP, $x_{i+1} - x_i$ vs $x_{i+2} - x_{i+1}$, for the six waves of cases can be seen in Fig. 7. In the 1st wave, most of the points fall within the circle with $R = 200$, where, according to Fig. 6, we have CTM$\approx$0.9, indicating low variability. This aligns with the first panel shown in Fig. 7. We can also compare it with Fig. 2 for $\tau = 1$, where we observe a high correlation in the PP, which directly implies low variability in the data. In terms of disease spread, within the considered radius, one can infer that the disease was spreading in a "controlled" velocity rate, reflecting the early stages of the pandemic in the city of Rio de Janeiro. The implementation of restrictive measures also played a role in reducing virus transmission among the population.

In the 2nd wave, the points are slightly more dispersed within the specified radius region, and there are also more points outside this region, indicating slightly higher variability compared to the 1st wave, with CTM ≈ 0.8, revealing lower variability. In terms of disease spread, one can infer that the virus transmission rate is spreading at a faster pace than in the first wave. In the 3rd wave, we continue to observe high variability. Comparing it with Fig. 6, in this case, we have CTM ≈ 0.825, slightly higher than the previous value (2nd wave). This is also captured in the PP (Fig. 2), where we see the presence of scattered points along the identity line and the formation of clusters.

In the 4th wave, the pattern of the SODP shows an interesting behavior. In this case, CTM ≈ 0.815, which is slightly lower than in the 3rd and 2nd waves, indicating a slight increase in data variability. This suggests that during the period considered in the 4th wave, the number of infected individuals is higher than in the previous waves. It is interesting to note that most of the scattered points are in the III quadrant of the plot. This suggests that although the number of infections is increasing compared to the previous waves (see Fig. 1(a)), it follows a decreasing pattern. In other words, despite the increased data variability, the number of cases starts to decrease.

The behavior of the 5th wave corroborates what was observed in the 4th wave. In this case, CTM ≈ 0.825, indicating lower variability compared to the previous wave, which strongly suggests that the number of cases is decreasing. It indicates a decrease in the virus's transmission rate. Finally, in the 6th wave, we have the lowest CTM value indicating high variability. After the decrease in the number of cases in the fifth wave, the number of infected individuals increases abruptly, resulting in an increase in the disease's transmission rate. Note that with the chosen radius of $R = 400$, few points fall within it. The presence of many points in the first quadrant reveals the increasing nature of the disease's transmission rate. This phenomenon can be observed in both time series (Fig. 1(a)) and the PP (Fig. 2). Remembering that in the 6th wave, the circulating variant was Omicron, known for its high transmission rate among individuals, which is consistent with the results presented.

The same analysis can be applied to the time series of deaths. In this case, the radius was set to $R = 10$ for all waves, which returns CTM values in the same range as we considered for the COVID-19 cases. By direct inspection of Fig. 8, we can see that the CTM values saturate for much smaller radii, even for the 6th wave, with $R > 20$. The CTM curve increases monotonically for all waves, indicating that the CTM value does not vary significantly from one wave to another.

Fig. 9 shows that for the 1st wave, there is high variability among the points, as seen in Fig. 8, with CTM ≈ 0.7, which may indicate a high number of deaths caused by the disease during that period (see Fig. 1(b)). In the 2nd wave, CTM ≈ 0.25, indicating fewer points outside the region defined by the radius, suggesting lower variability compared to the 1st wave. During the 3rd wave, there is a slight increase in variability, as evidenced by a greater number of points outside the defined radius. The 4th and 5th waves have the same CTM value for all considered radii. By analyzing the SODP, most points fall in the third quadrant, indicating a decrease in the number of deaths in the following wave, which is supported by the time series of deaths (see Fig. 1(b)). However, in the 5th wave, many points fall on the horizontal and vertical lines, which is an indication that the number of deaths continues to decrease at a high rate.

Finally, in the 6th wave, almost all points fall within the region defined by the radius. Therefore, the time series for the considered period exhibits low variability, with CTM ≈ 0.75. Analyzing both the time series (Fig. 1(b)) and the PP (Fig. 3), we can see that indeed the 6th wave has the lowest number of deaths during the analyzed period of the COVID-19 pandemic. Similarly to the cases analysis, during this period, the Omicron variant was present, which, in addition to its high transmission rate, is characterized by lower lethality. It is worth noting that during the 6th wave, a significant portion of the population had acquired immunity to the virus and its variants, either through previous infection or as a result of the high vaccination coverage in the city of Rio de Janeiro.

4. Conclusion

In this study, we conducted an analysis of the time series data for COVID-19 cases and deaths in Rio de Janeiro city from March 27, 2020 up to September 9, 2022. Through the techniques employed, we were able to identify the dynamic behavior of

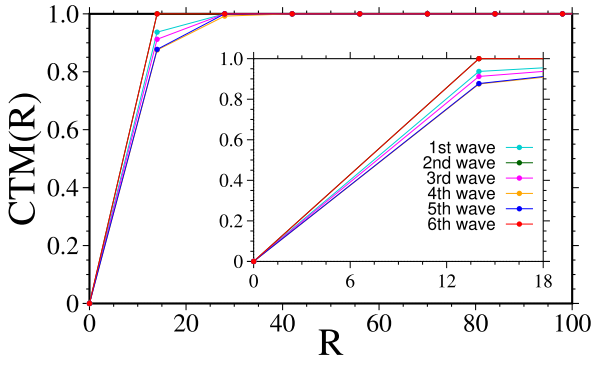

Fig. 8. Variation of CTM by radius for time series of deaths. As R increases, all waves tend towards CTM = 1, the same behavior presented for the case time series.

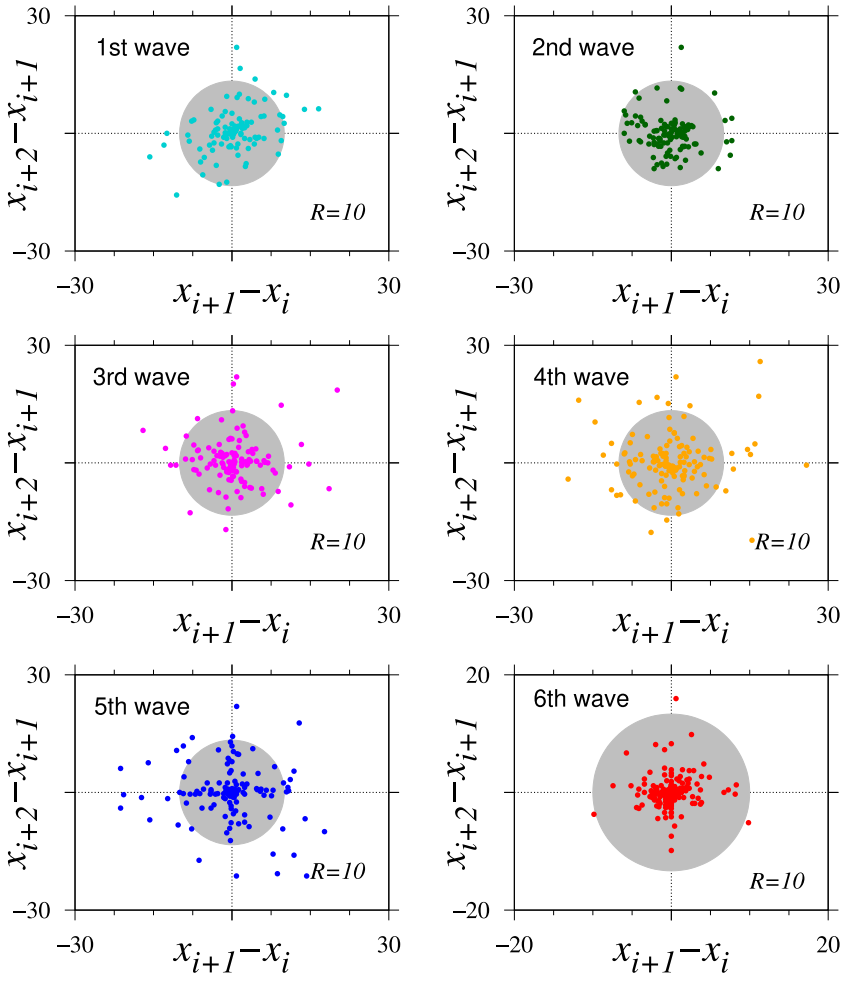

Fig. 9. CTM and second-order difference plot for the six waves of COVID-19 deaths. The figure captures the deceleration in the number of daily deaths.

the virus spreading shown in the time series using Poincaré plot, approximate entropy, second-order difference plot and central tendency measures. Both for cases and deaths time series, the calculated values for the descriptors adequately reflect the behavior in the Poincaré plot, corroborating the evolution of the multiple waves of COVID-19. The agreement between the descriptors and the visual representation in the Poincaré plot reinforces the analysis of the waves and contributes to a better understanding of the dynamics of COVID-19. By entropy analysis, we capture the level of complexity of each wave, caused by each variant, in circulation in the considered period.

The analysis of time series of epidemiological diseases using Poincaré Plot, approximate entropy, central tendency measure, and second-order difference plot is a new approach in terms of understanding the dynamics of these diseases. The advantage of using this set of techniques to interpret this type of data is that they are simple tools and provide a good understanding of the evolution of the spread of the disease, even allowing to capture the effects of the various mutations of the virus (different variants), measured restrictions and vaccination campaign. A limitation of this analysis is that, in general, those data present many fluctuations, as it depends on the correct completion of the necessary information by health agents, and the veracity and precision of the information provided by infected individuals. Another factor important to highlight is the period over which the data series were collected. A time series with more points would provide a greater interval for evaluating the results, providing slightly more robust results. However, since our interest was to characterize the dynamics of the virus within each wave, the evaluation interval considered proved to be adequate since the results obtained are close to what was observed during the pandemic.

Moreover, our results lead us to conclude that in the city of Rio de Janeiro, the Gamma variant was responsible for the highest number of deaths in relation to the number of infected individuals during the pandemic. Second-order difference plot and central tendency measure techniques reveal the speed of virus spread. By examining the structure, patterns, and properties of the time series, using the set of techniques cited in this paper, we got a better understanding of the epidemic spread, identify underlying dynamics, and extract meaningful information about the dynamical behavior of the time series.

Since our results are close to the true scenario during the COVID-19 pandemic in the city of Rio de Janeiro, these methods can be applied as a useful tool for analyzing time series of epidemiological diseases, alongside its existing applications in HRV and EGC analysis.

Funding

This study was financed in part by the Coordenação de Aperfeiçoamento de Pessoal de Nível Superior - Brasil (CAPES) - Finance Code 001 (88887.712553/2022–00), Conselho Nacional de Desenvolvimento Científico e Tecnológico - Brasil (CNPq) under grant 441016/2020-0 and São Paulo Research Foundation (FAPESP) under grant 2021/10599-3.

Availability of data and material

The data used in this study are available for download at http://coronavirus.rio/painel.

CRediT authorship contribution statement

Adriane S. Reis: Conceptualization, Data curation, Investigation, Methodology, Software, Validation, Visualization, Writing – original draft, Writing – review & editing. **Laurita dos Santos:** Conceptualization, Investigation, Methodology, Visualization, Writing – original draft, Writing – review & editing. **Américo Cunha Jr:** Conceptualization, Methodology, Writing – original draft, Writing – review & editing. **Thaís C.R.O. Konstantyner:** Methodology, Writing – original draft, Writing – review & editing. **Elbert E.N. Macau:** Conceptualization, Methodology, Resources, Supervision, Writing – original draft, Writing – review & editing.

Declaration of competing interest

The authors declare that they have no known competing financial interests or personal relationships that could have appeared to influence the work reported in this paper.

References

Abásolo, D., Hornero, R., Gómez, C., García, M., & López, M. (2006). Analysis of eeg background activity in alzheimer's disease patients with lempel–ziv complexity and central tendency measure. *Medical Engineering & Physics, 28*, 315–322.

Altan, G., Kutlu, Y., & Yeniad, M. (2019). Ecg based human identification using second order difference plots. *Computer Methods and Programs in Biomedicine, 170*, 81–93.

Belfort, R. E. A., Treccossi, S. P., Silva, J. L., Pillat, V. G., Freitas, C. B., & dos Santos, L. (2019). Extended central tendency measure and difference plot for heart rate variability analysis. *Medical Engineering & Physics, 74*, 33–40.

Brennan, M., Palaniswami, M., & Kamen, P. (2001). Do existing measures of Poincaré plot geometry reflect nonlinear features of heart rate variability? *IEEE Transactions on Biomedical Engineering, 48*, 1342–1237.

Brennan, M., Palaniswami, M., & Kamen, P. (2002). Poincaré plot interpretation using a physiological model of hrv based on a network of oscillators. *American Journal of Physiology - Heart and Circulatory Physiology, 238*, H1873–H1886.

Campos, F. C. C.d., & Canabrava, C. M. (2020). O Brasil na UTI: Atenção hospitalar em tempos de pandemia. *Saúde em Debate, 44*, 146–160.

Chen, X., Xu, G., Du, C., Zhang, S., Zhang, X., & Teng, Z. (2022). Poincaré plot nonextensive distribution entropy: A new method for electroencephalography (EEG) time series. *Sensors, 22*.

Cohen, M., Hudson, D., & Deedwania, P. (1996). Applying continuous chaotic modeling to cardiac signal analysis. *IEEE Engineering in Medicine and Biology Magazine, 15*, 97–102.

Delgado-Bonal, A., & Marshak, A. (2019). Approximate entropy and sample entropy: A comprehensive tutorial. *Entropy, 21*.

dos Santos, L., Barroso, J. J., Macau, E. E., & de Godoy, M. F. (2013). Application of an automatic adaptive filter for heart rate variability analysis. *Medical Engineering & Physics, 35*, 1778–1785.

dos Santos, L., Barroso, J. J., Macau, E. E., & de Godoy, M. F. (2015). Assessment of heart rate variability by application of central tendency measure. *Medical, & Biological Engineering & Computing, 53*, 1231–1237.

EpiRio. (2023). *Painél Rio Covid-19*. http://coronavirus.rio/painel. (Accessed 1 July 2023).

Facioli, T. P., Philbois, S. V., Gastaldi, A. C., Almeida, D. S., Maida, K. D., Rodrigues, J. A. L., Sánchez-Delgado, J. C., & Souza, H. C. D. (2021). Study of heart rate recovery and cardiovascular autonomic modulation in healthy participants after submaximal exercise. *Scientific Reports, 11*.

Gianfelice, P. R.d. L., Sovek Oyarzabal, R., Cunha, Americo, J., Vicensi Grzybowski, J. M., da Conceição Batista, F., & Macau, E. N. (2022). The starting dates of COVID-19 multiple waves. *Chaos: An Interdisciplinary Journal of Nonlinear Science, 32*, Article 031101.

Giovanetti, M., Slavov, S. N., Fonseca, et al. (2022). Genomic epidemiology of the SARS-CoV-2 epidemic in Brazil. *Nature Microbiology, 7*, 1490–1500.

Henriques, T., Ribeiro, M., Teixeira, A., Castro, L., Antunes, L., & Costa-Santos, C. (2020). Nonlinear methods most applied to heart-rate time series: A review. *Entropy, 22*.

Hsu, C. H., Tsai, M. Y., Huang, G. S., Lin, T. C., Chen, K. P., Ho, S. T., Shyu, L. Y., & Li, C. Y. (2012). Poincaré plot indexes of heart rate variability detect dynamic autonomic modulation during general anesthesia induction. *Acta Anaesthesiologica Taiwanica, 50*, 12–18.

Karmakar, C. K., Khandoker, A. H., Gubbi, J., & Palaniswami, M. (2009). Complex correlation measure: A novel descriptor for Poincaré plot. *BioMedical Engineering Online, 8*, 1–12.

Koichubekov, B., Riklefs, V., Sorokina, M., Korshukov, I., Turgunova, L., Laryushina, Y., Bakirova, R., Muldaeva, G., Bekov, E., & Kultenova, M. (2017). Informative nature and nonlinearity of lagged Poincaré plots indices in analysis of heart rate variability. *Entropy, 19*.

Kolmogorov, A. N. (1959). Entropy per unit time as a metric invariant of automorphism. *Doklady of Russian Academy of Sciences, 124*, 754–755.

Magno, L., Rossi, T. A., Mendonça-Lima, F. W.d., Santos, C. C.d., Campos, G. B., Marques, L. M., Pereira, M., Prado, N. M.d. B. L., & Dourado, I. (2020). Desafios e propostas para ampliação da testagem e diagnóstico para COVID-19 no Brasil. *Ciência & Saúde Coletiva, 25*, 3355–3364.

Ministério da Saúde. (2021). Informe semanal: Variantes de Atenção SARS-CoV-2. https://www.gov.br/saude/pt-br/coronavirus/informes-tecnicos/informes-de-variantes. (Accessed 1 July 2023).

Ministério da Saúde. (2023). Informe Semanal n°37 de Evidências sobre Variantes de Atenção de SARS-CoV-2. https://www.gov.br/saude/pt-br/coronavirus/informes-tecnicos/informes-de-variantes. (Accessed 1 July 2023).
Mohseni, M., Redies, C., & Gast, V. (2022). Approximate entropy in canonical and non-canonical fiction. *Entropy, 24*.
Moura, E. C., Cortez-Escalante, J., Cavalcante, F. V., Barreto, I. C.d. H. C., Sanchez, M. N., & Santos, L. M. P. (2022). Covid-19: Temporal evolution and immunization in the three epidemiological waves, Brazil, 2020–2022. *Revista de Saúde Pública, 56*, 105.
PGE-RJ. (2020). *Diário oficial do estado do Rio de Janeiro*. https://pge.rj.gov.br/covid19/estadual/decretos. (Accessed 1 July 2023).
Pincus, S. M. (1991). Approximate entropy as a measure of system complexity. *Proceedings of the National Academy of Sciences of the U S A, 88*, 2297–2301.
Pincus, S. M., Gladstone, I. M., & Ehrenkranz, R. A. (1991). A regularity statistic for medical data analysis. *Journal of Clinical Monitoring, 7*, 335–345.
Pincus, S. M., & Goldberger, A. L. (1994). Physiological time-series analysis: What does regularity quantify? *American Journal of Physiology - Heart and Circulatory Physiology, 266*, H1643–H1656.
Satti, R., Abid, N. U. H., Bottaro, M., De Rui, M., Garrido, M., Raoufy, M. R., Montagnese, S., & Mani, A. R. (2019). The application of the extended Poincaré plot in the analysis of physiological variabilities. *Frontiers in Physiology, 10*.
Secretaria de Saúde do Rio de Janeiro. (2023). *Boletim epidemiológico dos casos de Covid-19 no Estado do Rio de Janeiro 2020 – 2021*. https://painel.saude.rj.gov.br/arquivos/Boletim_2020_2021_2611.pdf. (Accessed 1 July 2023).
Tulppo, M. P., Makikallio, T. H., Takala, T. E., Seppanen, T., & Huikuri, H. V. (1996). Quantitative beat-to-beat analysis of heart rate dynamics during exercise. *American Journal of Physiology, 271*, H244–H252.
World Health Organization. (2020). *Novel Coronavirus (2019-nCoV): Situation report, 1. Technical documents*. . (Accessed 18 June 2023).